RSC Advances

PAPER

View Article Online
View Journal | View Issue

Cite this: *RSC Adv.*, 2023, **13**, 1627

High capacity and fast removal of Cr(VI) by alkali lignin-based poly(tetraethylene pentamine-pyrogallol) sorbent†

Rufei Xing,[a] Yanxin Song,*[b] Tingting Gao,[c] Xiaoxia Cai,[a] Jinshui Yao,[a] Qinze Liu*[a] and Changbin Zhang[d]

In this work, a novel alkali lignin-based adsorption material, alkali lignin-based poly(tetraethylene pentamine-pyrogallol) (AL-PTAP), was prepared using a Mannich reaction and catechol-amine reaction for removal of Cr(VI). It was characterized by thermogravimetric analysis (TGA), scanning electron microscopy (SEM), Fourier transform infrared spectroscopy (FT-IR) and X-ray photoelectron spectroscopy (XPS). The effects of tetraethylene pentamine (TEPA) dosage, pyrogallol (PL) dosage, contact time, pH, temperature and other factors on the adsorption behavior of the adsorbent were systematically investigated. These experimental data show that the adsorption behavior conforms to the pseudo-second-order kinetic model and the Langmuir isotherm model. The maximum adsorption capacity is 769.2 mg g^{-1} at 303 K, which is much higher than that of alkali lignin (AL). AL-PTAP can achieve a removal rate of almost 100% for Cr(VI) solutions with a concentration of less than 90 mg L^{-1} at 1 min. Furthermore, the toxic Cr(VI) is partly reduced to nontoxic Cr(III) during the adsorption process. Therefore, AL-PTAP is a fast and efficient alkali lignin-based adsorbent, which is expected to improve the utilization value of alkali lignin in Cr(VI) wastewater treatment.

Received 10th November 2022
Accepted 21st December 2022

DOI: 10.1039/d2ra07143f

rsc.li/rsc-advances

1. Introduction

Nowadays, water availability is a function of social, economic, environmental and political factors.[1,2] However, the pollution of water by heavy metals is increasingly serious, posing a threat to environmental safety and human health.[3,4] Among a large number of highly toxic metals, chromium is one of the most harmful metals, which comes from industrial processes such as steel making, leather tanning, metal coating, and plastics.[5,6] In water environment, chromium exists mainly in the form of trivalent Cr(III), which plays an important role in regulating glucose metabolism in the human body and hexavalent Cr(VI), which can cause serious harm to the human body and the environment.[7,8] The Cr(VI) ions in industrial wastewater are listed as the most carcinogenic substances by the International Agency for Research and the development of promising water purification technologies to deal with Cr(VI) ion contamination has attracted great attention.[9,10] Various methods have been used to solve the problem of Cr(VI) pollution, such as chemical precipitation, photoreduction,[11] ion exchange,[12] adsorption,[6] electrochemistry,[13] membrane filtration[14] and other methods. Among them, the adsorption method is considered to be an economical, environmentally friendly, simple and efficient method, which has a wide range of applications.[15]

Oxygen- and nitrogen-containing functional groups are the main adsorption groups in the adsorption process of Cr(VI) and the electrostatic adsorption of acid-based anions by protonated amino groups under acidic conditions enhance the adsorption capacity for Cr(VI).[16] Polydopamine is formed by self-polymerization of dopamine in Tris buffer (pH = 8.5), which is rich in hydroxyl and amino groups and has good adsorption capacity for heavy metal ions.[17] Inspired by the polymerization of dopamine, the poly(catechol-amine) (PCA) material, which contains abundant amino groups and hydroxyl groups, is easy to prepare, inexpensive and has good adsorption properties for Cr(VI). For example, Liu *et al.*[18] prepared poly(tannin-hexamethylenediamine) by catechol-amine reaction using tannic acid and hexamethylenediamine in alkaline solution, and the adsorption capacity of Cr(VI) could reach 283.29 mg g^{-1}. The poly(catechol-amine) (PCA) material, which contains abundant amino groups and hydroxyl groups, is easy to prepare,

[a]*School of Materials Science and Engineering, Qilu University of Technology (Shandong Academy of Sciences), #3501 Daxue Road, Western University Science Park, Jinan 250353, Shandong Province, P. R. China. E-mail: liuqinze@qlu.edu.cn; Tel: +86 13806410075*

[b]*School of Chemical Engineering & Pharmacy, Jining Technician College, #3166 Chongwen Road, Jining 272100, Shandong Province, P. R. China. E-mail: syxlhy001@163.com; Tel: +86 15668106398*

[c]*School of Chemistry and Chemical Engineering, Qilu University of Technology (Shandong Academy of Sciences), Jinan 250353, P. R. China*

[d]*Research Center for Eco-Environmental Sciences, Chinese Academy of Science, Beijing 100085, P. R. China*

† Electronic supplementary information (ESI) available. See DOI: https://doi.org/10.1039/d2ra07143f

inexpensive and has good adsorption properties for Cr(VI). Therefore, PCA materials were used to modify alkali lignin in this work.

Due to the consumption of traditional fossil energy and environmental pollution, more and more biomass materials are being used in various fields.[16,19–21] And lignin, which is the second most abundant biomass in nature, is one famous of these biomass materials. For example, Trano *et al.*[22] designed a lignin base membrane by cross-linking a pre-oxidized Kraft lignin matrix with an ethoxylated difunctional oligomer. This self-standing membranes are incorporate solvated potassium salts to utilize in potassium batteries with remarkable electrochemical properties. Goretti *et al.*[23] developed a flexible portable pressure sensor based on polyaniline (PANI)/lignin/acrylate photopolymer. Carlos *et al.*[24] proposed a novel biobased polyurethane (PU) coating with high lignin content which can be used as a high-performance bio-based material to replace traditional petroleum-based platforms. Tan *et al.*[25] synthesized biodegradable aerogel for Cr(VI) adsorption using pineapple leaves (PLs) and chitosan (CS) as raw materials with maximum absorption amount of 210.6–211.4 mg g^{-1}. Albadarin *et al.*[26] used alkali lignin to remove Cr(VI) with a maximum adsorption capacity of 31.6 mg g^{-1}. Song *et al.*[27] prepared a magnetic lignin composite with an equilibrium adsorption capacity of 123.0 mg g^{-1}. In the past few decades, lignin has received extensive attention as adsorbent to remove Cr(VI) ions from water.[28,29] However, these lignins and their derivatives have low adsorption performance. Therefore, it is of great significance to develop a lignin-based adsorbent with excellent adsorption capacity for Cr(VI).

Alkali lignin-based poly(tetraethylene pentamine-pyrogallol) (AL-PTAP) was prepared by reacting TEPA and formaldehyde with AL through Mannich reaction, then linking pyrogallol through catechol-amine reaction. The effects of various factors on the adsorption performance of the adsorbent were explored and the adsorption kinetics and isotherms were also investigated. The structure, thermal stability and adsorption properties of the materials were analyzed by SEM, TGA, UV, XPS and other characterization methods.

2. Experimental section

2.1. Chemicals

Alkali lignin was purchased from Energy Chemical (Shanghai, China). 95% tetraethylenepentamine solution, 37% formaldehyde aqueous solution, pyrogallol and potassium dichromate were supported by Macklin (Shanghai, China). Hydrochloric acid and sodium hydroxide were obtained from HengXing Chemical Reagent (Tianjin, China). 1,5-Diphenylcarbazide was purchased from Sinopharm Chemical Reagent Co. (Shanghai. China). Deionized water was used throughout the work (DW) (18.25 MV cm).

2.2. Preparation of AL-PTAP

The AL-PTAP was prepared by adjusting the ratio of the reactants, taking the AL-PTAP prepared under the condition that the TEPA/AL mass ratio was 0.8 : 1 and the TEPA/PL molar ratio was 2.5 : 1 as an example. 1.25 g of AL were dissolved in 100 mL of deionized water to form an alkali lignin solution. 1 g of TEPA was added, then the pH of the mixture was adjusted to 11. Formaldehyde was added dropwise and the mixture was stirred at 82 °C for 5 h. Then, it was cooled to room temperature and 1.66 g of PL were added to the mixture. This was further stirred for 72 h, then centrifuged and washed, and the samples were obtained by freeze-drying. Without other statement, AL-PTAP is that prepared under this condition (TEPA/AL mass ratio is 0.8 : 1, TEPA/PL molar ratio is 2.5 : 1). The preparation process of AL-PTAP and its possible reaction mechanism are shown in Fig. 1.

2.3. Characterizations

The surface morphology of the adsorbent was observed by scanning electron microscopy (SEM-EDX, ZEISS-Sigma 300, Germany). Fourier transform infrared spectrometer (FTIR, NICOLET iS10, USA) was used to record the specific functional groups of the adsorbent before and after adsorption. The thermal properties of the adsorbents before and after adsorption were tested by thermogravimetric analysis (TGA, Mettler Toledo, Switzerland). The elemental composition of the adsorbent was characterized by elemental analysis (EA, Elementar UNICUBE, Germany). The elemental composition of the adsorbent before and after adsorption was analyzed by X-ray photoelectron spectroscopy (XPS, ESCALAB Xi+, USA). The optical absorption of Cr(VI) solution was measured at a wavelength of 540 nm using an ultraviolet spectrophotometer (UV-2550, Shimadzu, Japan). BET specific surface area (S_{BET}) and Barrett–Joyner–Halenda (BJH) pore volumes (V_{BJH}) were determined by BET specific surface area analyzer (BET, ASAP2460, USA).

2.4. Batch adsorption experiments

The influence of various factors on the adsorption behavior of the adsorbent was explored by the controlled variable method, including the amount of tetraethylene pentamine, the amount of pyrogallol, the contact time (0–36 h), the initial concentration of Cr(VI) solution (90–320 mg L^{-1}), the temperature (293.15–313.15 K), the initial pH (2–7), the adsorbent dosage (15–55 mg). First, $K_2Cr_2O_7$ was dissolved in DW to prepare a Cr(VI) solution with a concentration of 2000 mg L^{-1}, then this solution was diluted to different concentrations of Cr(VI) solution. The pH of the Cr(VI) solution was adjusted by NaOH (1 mol L^{-1}) or HCl (1 mol L^{-1}). A certain amount of adsorbent and 100 mL of Cr(VI) solution were added to a 150 mL Erlenmeyer flask, which was then placed into a constant-speed (200 rpm) constant temperature shaker for shaking. After shaking, 1 mL of supernatant was collected by centrifugation and its concentration was analyzed by the 1,5-diphenylcarbazide method[30] at 540 nm using an ultraviolet spectrophotometer. All the data were obtained by averaging the average of three repeated experiments.

The adsorption capacity and removal rate of Cr(VI) by AL-PTAP can be estimated by the following equations

$$Q_e = (C_0 - C_e)V/m \quad (1)$$

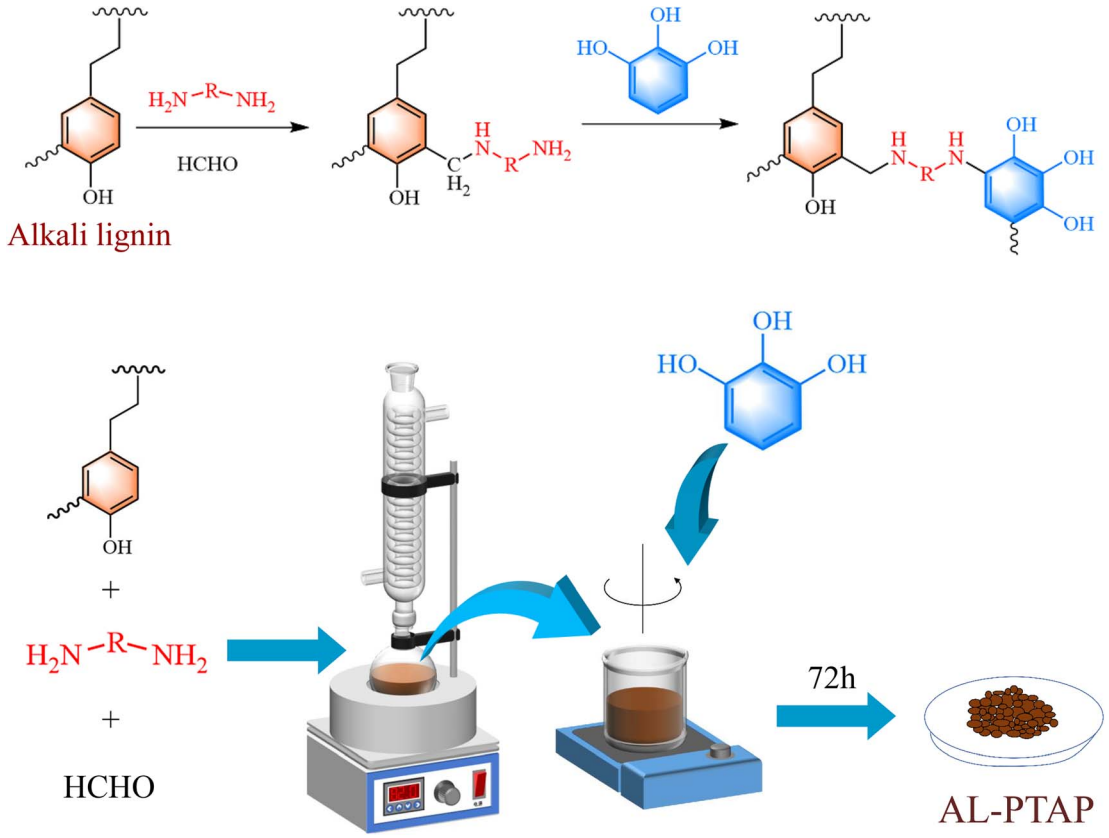

Fig. 1 Schematic diagram of preparation process of AL-PTAP and possible reaction mechanism.

$$Q_t = (C_0 - C_t)V/m \quad (2)$$

$$R\% = (C_0 - C_t)/C_0 \times 100\% \quad (3)$$

where Q_e (mg g^{-1}) and Q_t (mg g^{-1}) are the adsorption capacity of the adsorbent at adsorption equilibrium and the adsorption capacity at any time, respectively. C_0 (mg L^{-1}) and C_e (mg L^{-1}) are the initial and equilibrium concentrations of the Cr(VI) solution, respectively, and C_t (mg L^{-1}) is the concentration of the Cr(VI) solution at any time. m (g) and V (L) are the mass of AL-PTAP and the volume of Cr(VI) solution, respectively. R (%) is the removal rate.

3. Results and discussion

3.1. Characterization of AL-PTAP

The surface morphologies of AL and AL-PTAP were studied using SEM and shown in Fig. 2. AL is a large particle size with irregular structure (in Fig. 2a). Its surface is smooth. Compared with AL, the shape of AL-PTAP (in Fig. 2c) was significantly changed, its size was reduced. It appears as a particle cluster made up of aggregates of nano-sized particles. These spherical particles give the adsorbent a large specific surface area, which may increase the adsorption capacity of the material for heavy metal ions. These changes in morphology of AL and AL-PTAP may indicate that the alkali lignin was dissolved and reconstituted during the reaction.

The SEM and EDS spectra of AL-PTAP before and after adsorption of Cr(VI) are shown in Fig. 2e and S1.† Compared with the image of AL-PTAP before adsorption Cr(VI), the presence of chromium element in the image after adsorption Cr(VI) indicated that AL-PTAP successfully adsorbed Cr(VI). Moreover, the surface morphology of AL-PTAP did not change significantly after adsorption of Cr(VI).

Table 1 summarizes the BET specific surface area (S_{BET}) and Barrett–Joyner–Halenda (BJH) pore volumes (V_{BJH}) of AL and AL-PTAP. These results show that S_{BET} and V_{BJH} of Al-PTAP are larger than those of AL which are proved in SEM images. Besides, the mesoporosity of Al-PTAP were confirmed by pore size distribution analysis (in Fig. S3†). These will provide more adsorption sites and increase the contact area between AL-PTAP and Cr(VI) to increase the adsorption property.

The FT-IR spectra of AL and AL-PTAP are shown in Fig. 3a. The peaks at 2935 cm^{-1} and 2850 cm^{-1} correspond to the C–H stretching vibrations of methyl and methylene in alkali lignin.[31] The peak at 1126 cm^{-1} is assigned to the C–O–C bond in alkali lignin.[32] The peak at 1039 cm^{-1} is attributed to aromatic C–N vibrations in alkaline lignin.[33] These characteristic peaks of lignin can be observed in both AL and AL-PTAP, which indicated that AL was successfully introduced into AL-PTAP. Compared with AL, new peaks in AL-PTAP are appeared at 1616 cm^{-1} and 1240 cm^{-1}, which can be attributed to N–H and C–N, respectively.[34,35] This indicates that AL has been aminated. The above results indicate the successful preparation of AL-PTAP.

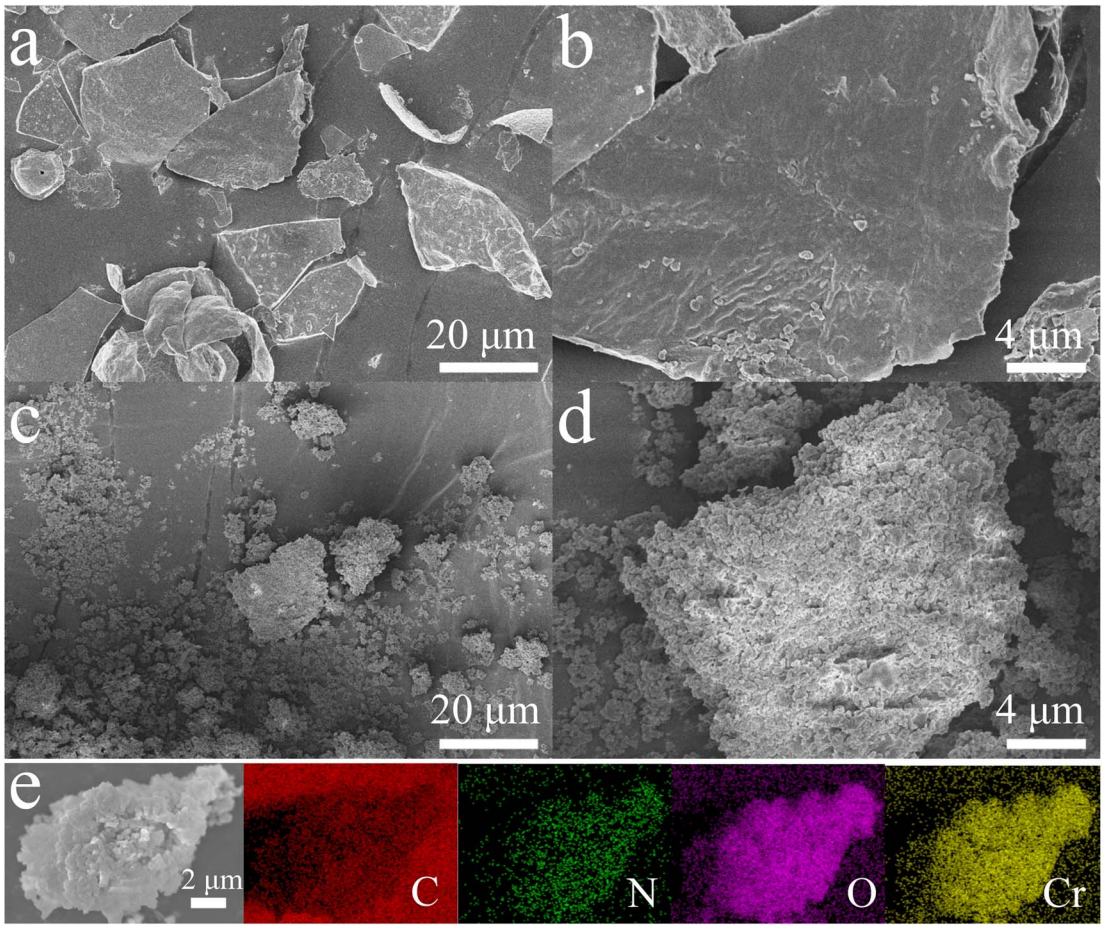

Fig. 2 (a and b) SEM images of alkali lignin; (c and d) SEM images of AL-PTAP; (e) EDS mappings of AL-PTAP after adsorption.

Table 1 Surface area and pore volume of AL and AL-PTAP

Sample	BET surface area ($m^2\ g^{-1}$)	BJH pore volume ($cm^3\ g^{-1}$)
AL	0.4924	0.000768
AL-PTAP	13.1338	0.046025

As it can be seen in Fig. 3b, after the adsorption of chromium on AL-PTAP, some IR peaks changed. The peak at 541 cm^{-1} in used AL-PTAP was attributed to Cr=O vibration, the peaks at 919 cm^{-1} and 821 cm^{-1} were caused by the phenolic hydroxyl groups interacting with Cr(VI). These results indicate that Cr(VI) was successfully adsorbed by AL-PTAP.

As shown in Fig. 3c, thermogravimetric analysis was used to characterize the thermal stability of the AL-PTAP, AL and PTAP under an air atmosphere. The thermogravimetric curves of AL and AL-PTAP are obviously different. The AL undergoes a water weight loss until 120 °C and two weight losses from 250 °C to 650 °C and 650 °C to 800 °C, with a residual rate of about 51%. AL-PTAP undergoes a water weight loss until 120 °C and has a large weight loss at 250 °C to 550 °C with a residual rate close to 0%. This is due to the reaction of AL with TEPA, which reduces intermolecular interactions.

The thermogravimetric curves of AL-PTAP before and after removal of Cr(VI) are shown in Fig. 3d. The weight loss rate of the curves before and after the removal of Cr(VI) by AL-PTAP is quite different, which indicates that a large amount of Cr(VI) are loaded on the adsorbent, the adsorbent has a higher adsorption capacity for Cr(VI). Compared with the curve of fresh AL-PTAP, the decomposition rate of the used AL-PTAP curve is faster, it drops rapidly at 260 °C and its complete decomposition temperature appears at 430 °C. The possible reason is that the π–π stacking and hydrogen bonds inside the adsorbent are weakened after adsorption, the intermolecular interaction force is reduced and the thermal stability of the used adsorbent is reduced.

3.2. Effect of ratio of TEPA/AL and TEPA/PL on adsorption capacity of adsorbent

In order to obtain adsorbents with higher adsorption capacity by controlling the input amount of reactants, the effects of TEPA/AL and TEPA/PL ratios on the adsorption capacity of adsorbents were investigated under the condition of constant formaldehyde dosage.

Fig. 4a shows the effect of the mass ratio of TEPA/AL in the preparation process on the adsorption amount. It can be seen

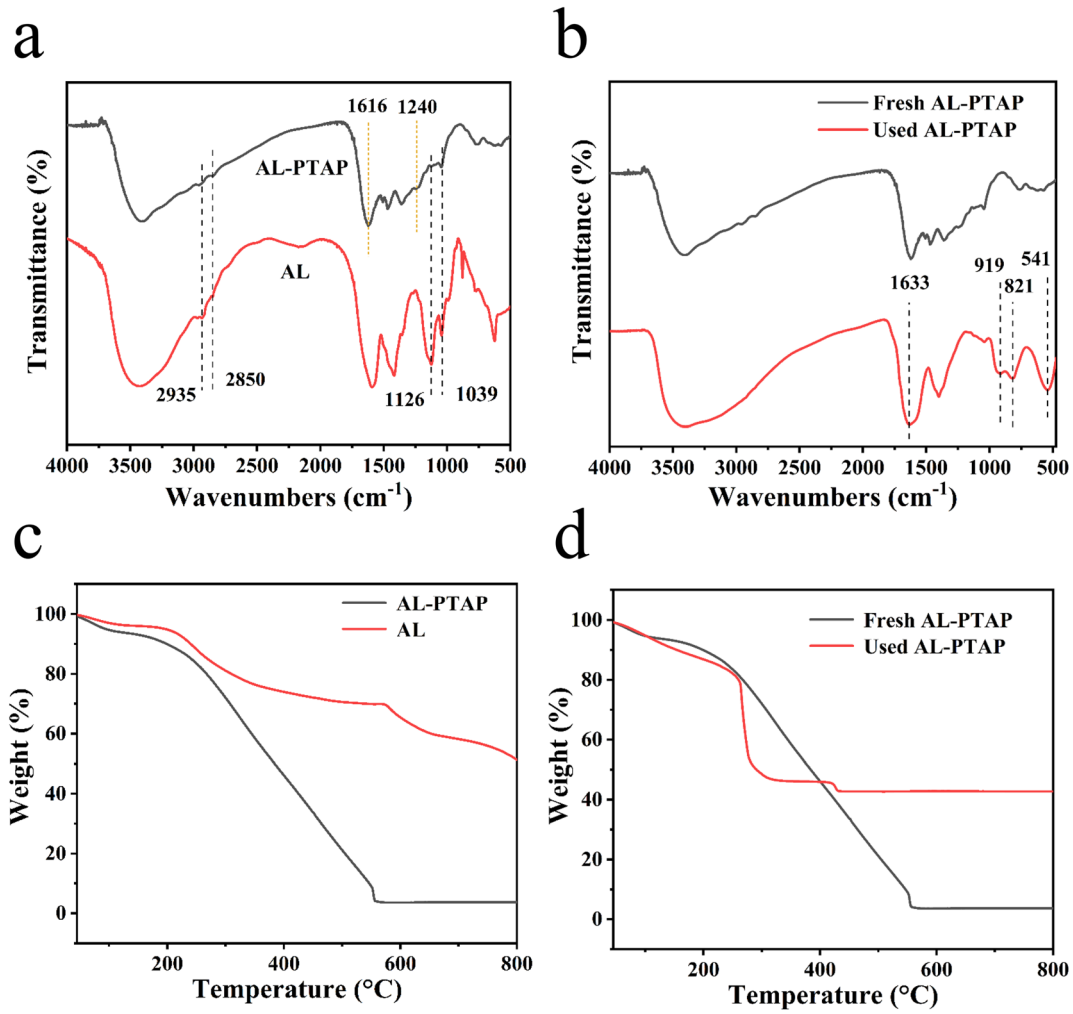

Fig. 3 (a) FTIR spectra for PTAP, AL and AL-PTAP; (b) FTIR spectra of AL-PTAP before and after adsorption of Cr(VI); (c) TG curves of PTAP, AL and AL-PTAP; (d) TG curves of AL-PTAP before and after adsorption of Cr(VI).

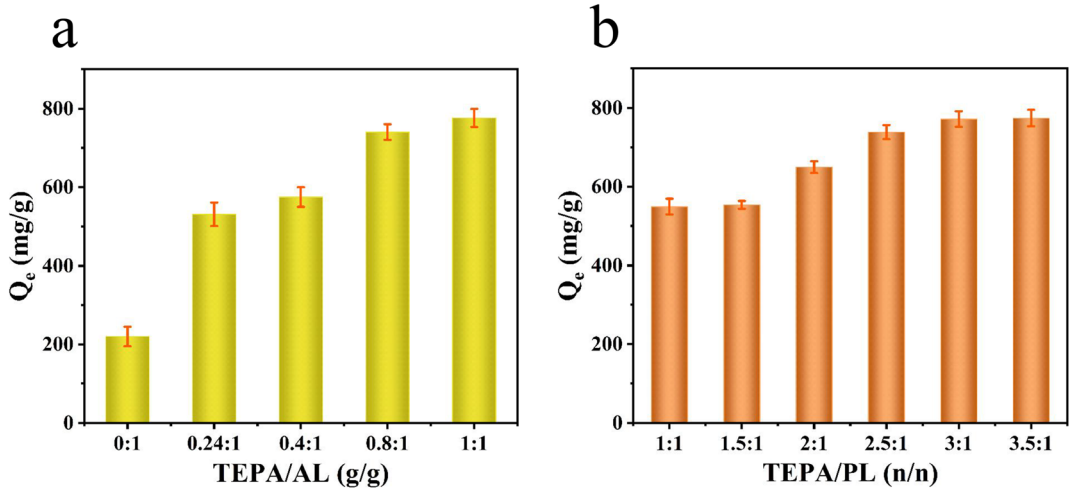

Fig. 4 (a) Effect of TEPA/AL mass ratio on adsorption performance of adsorbent; (b) effect of TEPA/PL molar ratio on adsorption performance of adsorbents.

Table 2 Effect of TEPA/AL ratio on elemental content of adsorbents

TEPA/AL (g g^{-1})	0 : 1	0.24 : 1	0.4 : 1	0.8 : 1	1 : 1
N content (%)	0.63	9.1	9.81	10.8	11.01

that the adsorption amount of AL is about 200 mg g^{-1}, which is much smaller than that of AL-PTAP. As the amount of TEPA is raised, the adsorption capacity gradually increases. When the TEPA/AL ratio is 1 : 1, the adsorption amount reaches 776.4 mg g^{-1}. This may be caused by the change in the number of amino groups (–NH–) due to the change in TEPA dosage. As it can be seen from Table 2, the N content of AL-PTAP was higher than that of AL, which indicates the successful introduction of TEPA. The N content increases following the increase of TEPA dosage. Therefore, it can be speculated that the increase in the amount of TEPA means that more TEPA is linked into AL-PTAP and the amount of amino groups (–NH–) in AL-PTAP increases. Besides, this means that the number of amino groups (–NH–) in the adsorbent plays an important role in the removal Cr(VI). When the mass ratio of TEPA/AL is 0.8 : 1 and 1 : 1, the difference in adsorption capacity is not much. Therefore, in order to reduce TEPA consumption and maintain large adsorption amount of AL-PTAP, the adsorbent was prepared when the mass ratio of TEPA/AL was 0.8 : 1.

Fig. 4b shows the adsorption performance of AL-PTAP with different TEPA/PL molar ratios prepared under the same conditions. It can be seen that the adsorption capacity of the adsorbent for Cr(VI) increases gradually with the increase of the PL ratio. When the ratio is 1 : 3.5, the adsorption amount reaches 774.4 mg g^{-1}. This could be caused by the change in the number of hydroxyl groups (–OH) due to the change in the PL dosage. From Table 3, it can be seen that the N content decreases and the atomic ratio of O : N increases when the PL dosage increases. Therefore, it can be speculated that when the dosage of PL increases, more PL reacts with the aminated lignin and the number of hydroxyl groups (–OH) in the adsorbent increases. It can be speculated that the adsorption performance of the adsorbent for Cr(VI) increases when the number of hydroxyl groups (–OH) in the adsorbent increases. When the molar ratio of TEPA/AL is 1 : 2.5, 3 : 1, 3.5 : 1, the difference in adsorption capacity is small. In order to make AL-PTAP have high adsorption capacity while reducing PL consumption, the TEPA/PL molar ratio of 2.5 : 1 was chosen to prepare the adsorbent.

According to the above analysis, it can be inferred that both the amino group (–NH–) and the phenolic hydroxyl group (–OH) play a role in the adsorption process of Cr(VI), and the adsorption performance of AL-PTAP increases when the number of these two groups increases.

Table 3 Effect of TEPA/PL ratio on elemental content of adsorbents

TEPA/PL (n/n)	1 : 1	1.5 : 1	2 : 1	2.5 : 1	3 : 1	3.5 : 1
N content (%)	13.29	12.49	11.67	10.8	10.73	10.54
O : N	1.9	2.06	2.51	2.53	2.61	2.67

3.3. Effect of contact time

The effect of contact time on the adsorption capacity of Cr(VI) is shown in Fig. 5a. The adsorption capacity of AL-PTAP for Cr(VI) can reach 456 mg g^{-1} at 5 min. This indicates that AL-PTAP can adsorb Cr(VI) in a large amount in a short time. This may be owed to that AL-PTAP has a large number of active sites in the initial stage, which have a high affinity for Cr(VI) and rapidly interact with Cr(VI). The growth rate of Q_t slowed down with time, which was due to the depletion of active sites in AL-PTAP and the interaction of AL-PTAP with Cr(VI). After 24 h, the adsorption capacity of Cr(VI) (703.2 mg g^{-1}) approached a constant value and reached the adsorption equilibrium.

To reveal the fast adsorption performance of AL-PTAP, different concentrations of Cr(VI) were adsorbed within 30 min (in Fig. 5b). The removal rate can reach almost 100% in 1 min when the Cr(VI) concentrations less than 90 mg L^{-1}. At 30 min, the removal rate of Cr(VI) with a concentration of 115 mg L^{-1} can reach 94.2% and the removal rate of Cr(VI) with a concentration of 200 mg L^{-1} can reach 72.1%. This excellent fast adsorption performance is attributed to the following synergistic effects: (1) AL-PTAP has a large number of active sites and these active sites quickly contact with Cr(VI) in a short time to achieve the effect of rapid adsorption of Cr(VI), (2) the spherical particle cluster structure of AL-PTAP makes it have a larger specific surface area, which increases the contact area of Cr(VI). In summary, AL-PTAP has great potential for ultrafast adsorption of Cr(VI).

3.4. Effect of Cr(VI) initial concentration

Fig. 6a shows the adsorption performance of AL-PTAP at different initial concentrations of Cr(VI). When the initial concentration of Cr(VI) was lower than 140 mg L^{-1}, the removal rate of Cr(VI) was close to 100%. When the initial concentration of Cr(VI) increased, the removal rate of Cr(VI) by AL-PTAP decreased and the increasing trend of adsorption capacity gradually became gentle, and the maximum adsorption capacity could reach 762.8 mg g^{-1}. This may be due to the limited active sites of AL-PTAP, which cannot provide enough active sites for the increased Cr(VI), resulting in a lower removal rate. The active sites of AL-PTAP were gradually occupied by sufficient Cr(VI) and AL-PTAP gradually reached the saturated adsorption state, resulting in a gradual increase in the adsorption capacity. AL-PTAP shows high removal efficiency for Cr(VI), adsorption amount about 560 mg g^{-1} with removal percentage nearly 100%, maximum adsorption capacity reaching 762.8 mg g^{-1}, which facilitates the application of this adsorbent in practical industrial pollution control.

3.5. Effect of initial pH

As shown in Fig. 6b, the initial pH of the Cr(VI) solution strongly affected the removal of Cr(VI) by AL-PTAP. The adsorption capacity reached the maximum value at pH = 2 and it decreased when the pH value increased. This is owed to that the initial pH of the Cr(VI) solution can affect the chemical species of Cr(VI)

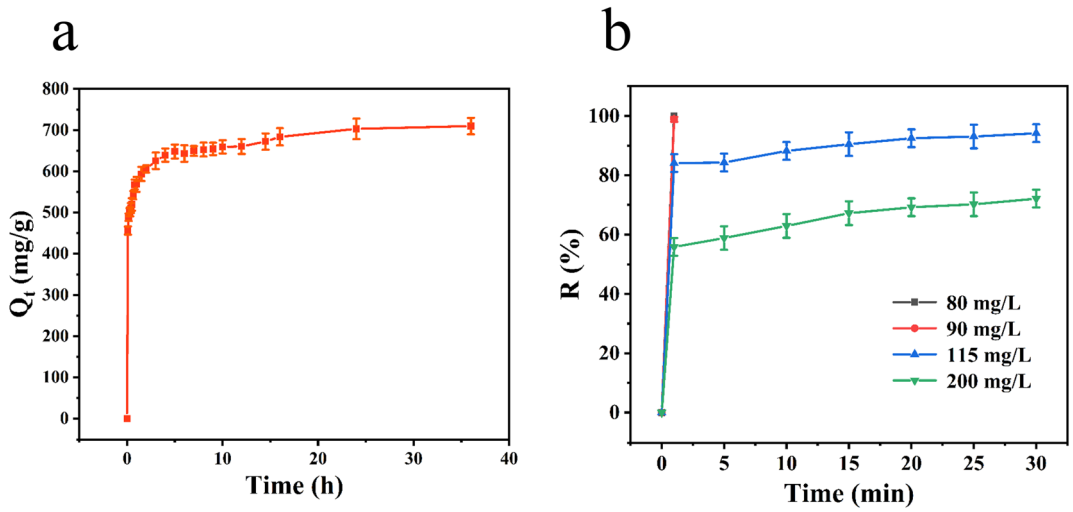

Fig. 5 (a) Effect of contact time (dos = 25 mg, C_0 = 280 mg L^{-1}, V = 100 mL, T = 30 °C, t = 0–36 h); (b) effect of contact time and initial concentration (dos = 25 mg, C_0 = 90–200 mg L^{-1}, V = 100 mL, T = 30 °C, t = 0–30 min).

and the functional groups in AL-PTAP.[36] At pH 2.0–6.0, the main form of Cr(VI) is $HCrO_4^-$, when the pH exceeds 6, the main form of Cr(VI) is CrO_4^{2-}.[37] In addition, when the pH condition is strongly acidic, the –NH– groups in Al-PTAP have a high degree of protonation and are easy to form $-NH_2^+$.[36] This would enhance the adsorption of $HCrO_4^-$ by AL-PTAP. When the pH of

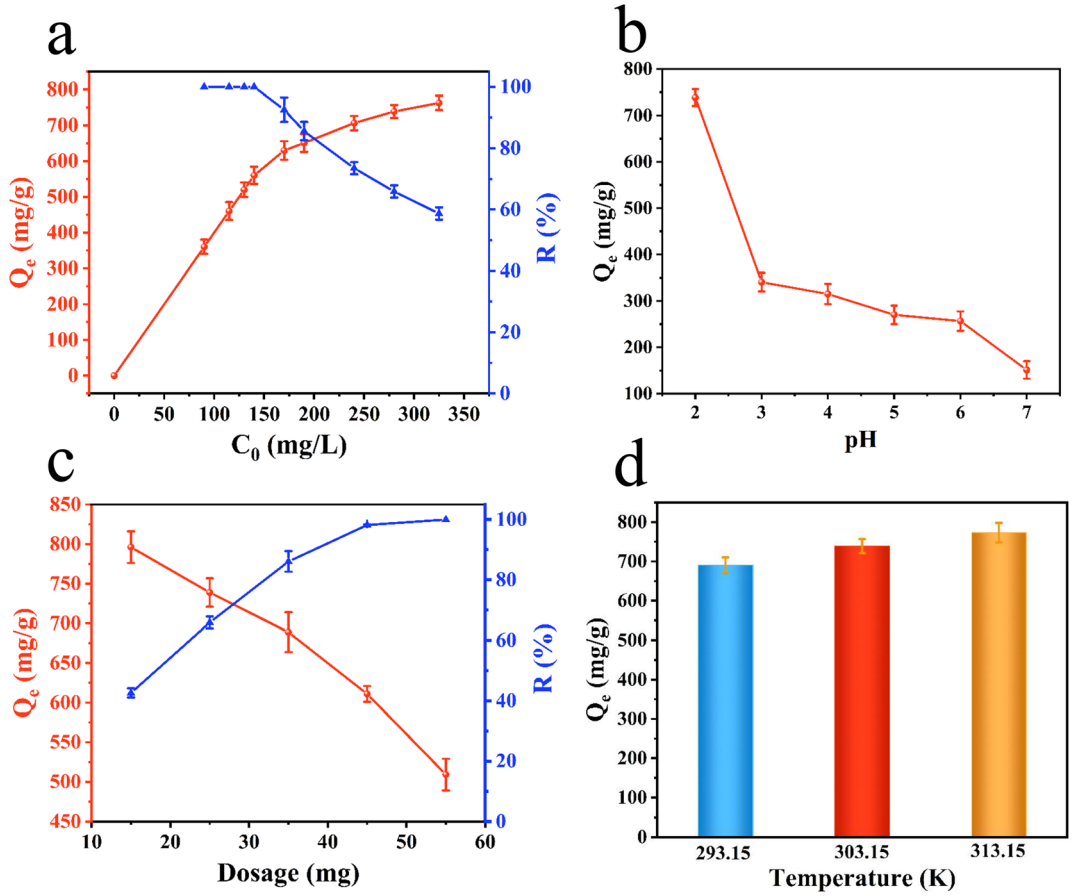

Fig. 6 Effect of (a) initial Cr(VI) concentration (condition: dose 0.025 g, initial Cr(VI) = 0–325 mg L^{-1}, pH = 2, 303.15 K, 24 h), (b) pH (condition: dose 0.025 g, initial Cr(VI) = 280 mg L^{-1}, pH = 2–7, 303.15 K, 24 h), (c) adsorbent dose (condition: dose 0.015–0.055 g, initial Cr(VI) = 280 mg L^{-1}, pH = 2, 303.15 K, 24 h), (d) temperature (condition: dose 0.025 g, initial Cr(VI) = 280 mg L^{-1}, pH = 2, 293.15–313.15 K, 24 h) on Cr(VI) adsorption by AL-PTAP.

Cr(VI) solution increased, the degree of protonation of –NH– groups decreased, resulting in a decrease in adsorption capacity. Therefore, the adsorption experiments were carried out under the condition of pH = 2.

3.6. Effect of adsorbent dose

Fig. 6c shows the effect of the initial dosage of adsorbent on the adsorption performance of AL-PTAP. The results showed that, with the increase of adsorbent dosage, the removal percentage increased. When the adsorbent dosage is 45 mg or 55 mg, the removal rate is close to 100%, which indicates that almost all Cr(VI) ions in the simulated wastewater have been removed. However, when the amount of adsorbent is too large, AL-PTAP does not reach its maximum saturated adsorption capacity and, if the amount of adsorbent is too high, active sites will not be utilized. The adsorption capacity decreases as the adsorbent dosage increases. This is because the ratio of active sites/Cr(VI) ions increases as the adsorbent dosage increases, the utilization decreases caused by too many active sites and the adsorption capacity per unit mass of adsorbent AL-PTAP decreases. Therefore, in order to make the adsorption process have a high adsorption capacity and a high removal rate, the optimal dosage for removing Cr(VI) is 25 mg.

3.7. Effect of temperature

As shown in Fig. 6d, the adsorption capacity of AL-PTAP for Cr(VI) increased with increasing temperature. Elevated temperature can increase the diffusion rate of metal ions, increase the collision probability between active sites and Cr(VI), promote the effective binding of active sites to Cr(VI). These factors will increase the utilization of active sites in AL-PTAP and increase the adsorption capacity. The adsorption thermodynamic parameters are calculated and shown in Fig. S2 and Table S1† ($\Delta G < 0$, $\Delta H > 0$). The above results indicate that the adsorption process is spontaneous and endothermic in nature, where the adsorption of Cr(VI) on AL-PTAP is mainly chemical adsorption. AL-PTAP can maintain a high adsorption capacity for Cr(VI) in the temperature range of 293.15–313.15 K.

3.8. Adsorption kinetic models

Adsorption kinetics is an important aspect to analyze the adsorption process and mechanism. In order to study the

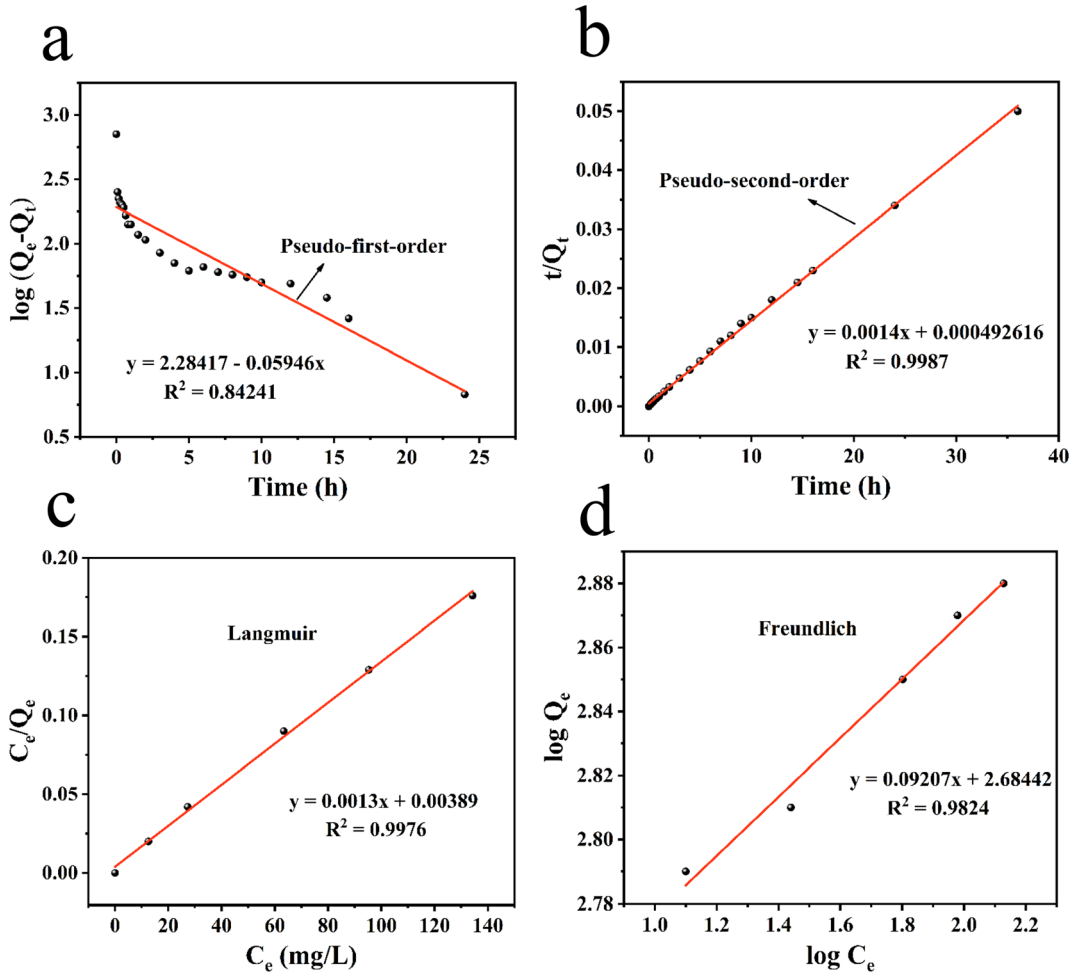

Fig. 7 (a) Pseudo-first-order kinetic model, (b) pseudo-second-order kinetic model, (c) Langmuir model, (d) Freundlich model of Cr(VI) removal by AL-PTAP.

adsorption kinetics mechanism, the experimental data were fitted and analyzed based on the pseudo-first-order kinetic model and the pseudo-second-order kinetic model. The mathematical expressions of the pseudo-first-order and pseudo-second-order dynamic models are expressed as follows, respectively:

Pseudo-first-order kinetic model:[38]

$$\log(Q_e - Q_t) = \log Q_e - k_t/2.303 \quad (4)$$

Pseudo-second-order kinetic model:[39]

$$t/Q_t = 1/(k_2 Q_e^2) + t/Q_e \quad (5)$$

where Q_e (mg g^{-1}) and Q_t (mg g^{-1}) are the adsorption capacities of Cr(VI) at equilibrium and at time t, respectively. k_1 (h^{-1}) and k_2 (g mg^{-1} h^{-1}) are pseudo-first-order kinetic rate constants and pseudo-second-order kinetic rate constants, respectively.

The data fitting results are shown in Fig. 7a and b and Table 3. It can be found that the correlation coefficient ($R^2 = 0.9987$) of the pseudo-second-order model is higher than that of the pseudo-first-order model ($R^2 = 0.84241$), while the Q_e value (714.3 mg g^{-1}) calculated by the pseudo-second-order model is close to the experimental date. Therefore, the pseudo-second-order model is more suitable to describe the adsorption of Cr(VI) on AL-PTAP. These results suggest that chemisorption is the rate-limiting step in the pseudo-second-order model.

3.9. Adsorption isotherm models

The adsorption isotherm model describes the relationship between the adsorption amount Q_e of Cr(VI) by AL-PTAP at constant temperature and the residual concentration C_e at equilibrium. The isotherm adsorption model is of great significance for exploring the isotherm adsorption process and the adsorption mechanism of Cr(VI) on AL-PTAP. The Langmuir and Freundlich isotherm models were applied to fit the experimental data. Among them, the Langmuir model assumes that adsorption may only occur on a fixed number of local sites on the surface, all adsorption sites on these sites are identical and energy equivalent, and the adsorption process is a monolayer adsorption mechanism.[40] The Freundlich model assumes that the energy of the adsorbent surface and active site is not uniform.[41] The linear expressions of the Langmuir model and the Freundlich model are as follows:

Langmuir isotherm model:

$$\frac{C_e}{Q_e} = \frac{1}{K_L Q_m} + \frac{C_e}{Q_m} \quad (6)$$

Freundlich isotherm model:

$$\log Q_e = \log K_F + \frac{1}{n} \log C_e \quad (7)$$

where C_e (mg L^{-1}) is the concentration of Cr(VI) in the solution at equilibrium. Q_m (mg g^{-1}) and Q_e (mg g^{-1}) are the maximum adsorption capacity and equilibrium adsorption capacity, respectively. K_L is the Langmuir adsorption equilibrium constant related to binding site affinity. K_F is the Freundlich constant related to the adsorption capacity.

The fitting results of the two isotherm models are shown in Fig. 7c and d and Table 4. The correlation coefficient of the Langmuir model ($R^2 = 0.9976$) was better than that of the Freundlich model ($R^2 = 0.984$) and the equilibrium adsorption capacity (769.2 mg g^{-1}) calculated by the Langmuir model was closer to the experimental data. This indicates that the Langmuir model can better fit the adsorption process of Cr(VI) by AL-PTAP and it also indicates that the adsorption process is monolayer adsorption.

3.10. Adsorption mechanism analysis

To further study the adsorption behavior of Cr(VI) on AL-PTAP, X-ray photoelectron spectroscopy (XPS) was used to analyze the basic composition of AL-PTAP adsorbent before and after Cr(VI) removal. As it can be seen in Fig. 8a, a Cr 2p peak was observed in the used AL-PTAP, proving that chromium was successfully loaded into AL-PTAP. As it can be seen in Fig. 8b, the spectrum of Cr 2p includes two main peaks with binding energies of 577.5 and 587.3 eV, corresponding to the Cr $2p_{3/2}$ transition and the Cr $2p_{1/2}$ transition, respectively. The Cr 2p spectrum was subjected to peak analysis. Among them, the two larger peaks with binding energies of 577.3 and 587.1 eV correspond to the characteristic peaks of Cr(III),[42] while the two smaller peaks with binding energies of 588.9 and 579.5 eV are attributed to Cr(VI).[43] Part of Cr(VI) was reduced to less toxic Cr(III), Cr(III) and Cr(VI) coexisted on the surface of AL-PTAP after adsorption.

Fig. 8c shows the fine spectra of N 1s in AL-PTAP before and after Cr(VI) adsorption. The peak of fresh AL-PTAP can be attributed to –NH– (399.8 eV) and C–N (399.0 eV).[44] The peak of used AL-PTAP shifted to left that can be attributed to $–NH_2^+–$

Table 4 Parameters of the adsorption kinetic and isotherm models on adsorption of Cr(VI) ions by AL-PTAP

Models	Parameters		
Pseudo-first-order kinetic model	K_1 (h^{-1})	Q_e (mg g^{-1})	R^2
	0.1369	192.4	0.84241
Pseudo-second-order kinetic model	K_2 (g mg^{-1} h^{-1})	Q_e (mg g^{-1})	R^2
	0.00398	714.3	0.9987
Langmuir isotherm model	K_L (L mg^{-1})	Q_m (mg g^{-1})	R^2
	0.3342	769.2	0.9976
Freundlich isotherm model	K_F (mg g^{-1})/(mg L^{-1})	$1/n$	R^2
	483.5	0.09207	0.9824

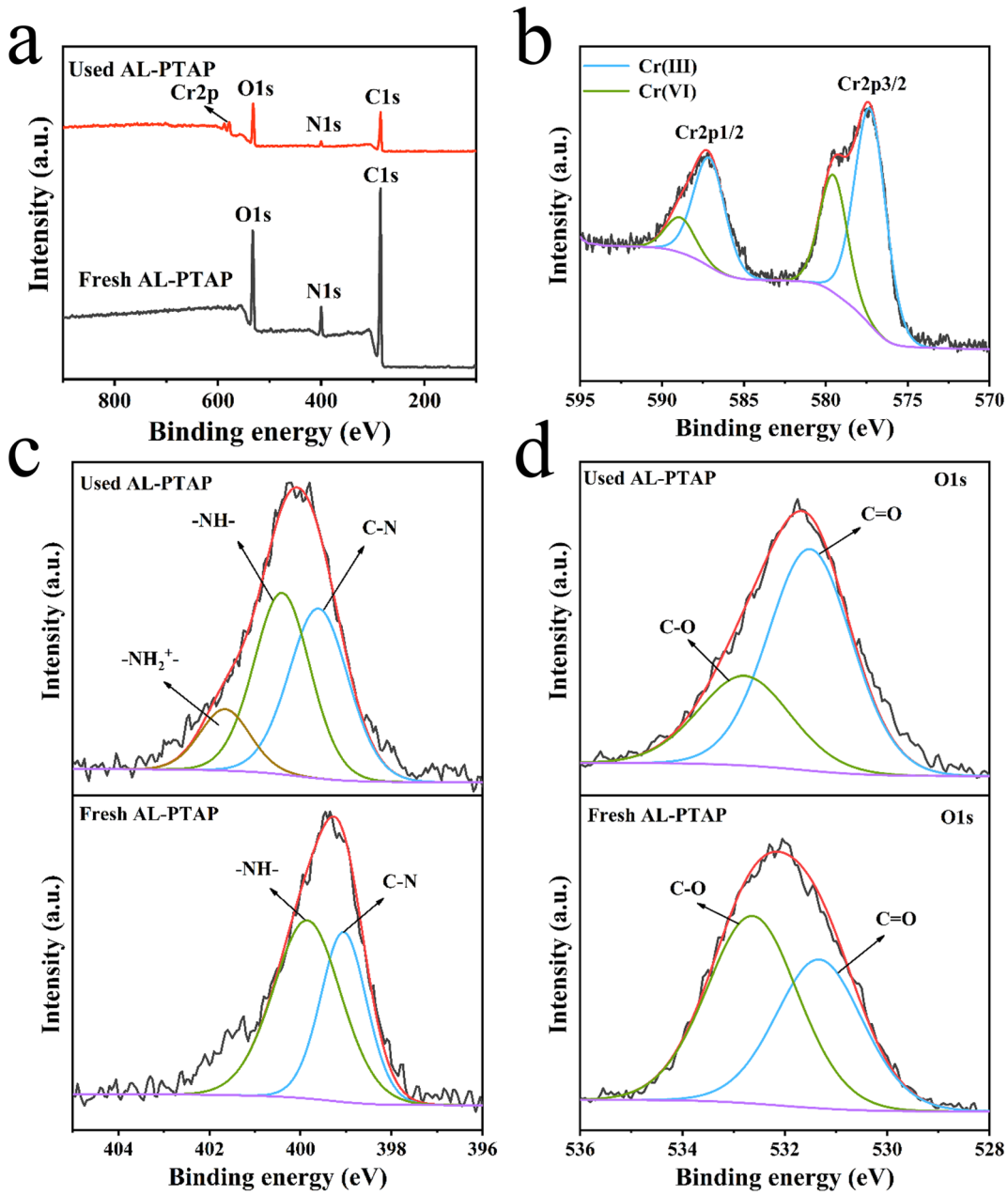

Fig. 8 (a) XPS spectra of fresh and used AL-PTAP; (b) XPS Cr 2p spectrum of used AL-PTAP; XPS spectra of fresh and used AL-PTAP: (c) N 1s, (d) O 1s.

(401.6 eV), which is formed by protonation under acidic conditions and helpful to adsorb Cr(VI) through electrostatic interactions.[45] Furthermore, Fig. 8d shows the O 1s fine spectra before and after Cr(VI) adsorption by AL-PTAP. The peaks with binding energies of 532.6 and 531.3 eV correspond to C–O and C=O, respectively. The relative intensity of the C=O bond peak in the used AL-PTAP increases. This may be because part of the C–OH groups are oxidized to C=O during the adsorption process and the C–OH groups may donate electrons for the reduction of Cr(VI) to Cr(III).[46] The above results indicate that both amine groups and hydroxyl groups in AL-PTAP play important roles in the adsorption process of Cr(VI). AL-PTAP could partly convert Cr(VI) to Cr(III) through the synergistic effect of electrostatic adsorption and chemical reduction. The possible mechanism of Cr(VI) adsorption by AL-PTAP is shown in Fig. 9.

3.11. Effects of competing ions

Since various anions and metal ions coexist with Cr(VI) in wastewater, it is of great significance to study the adsorption capacity of AL-PTAP for Cr(VI) in water containing competing ions. The effects of the presence of several common metal ions and anions on the adsorption performance of AL-PTAP for Cr(VI) were investigated. As shown in Fig. 10a, Cu^{2+} ions, K^{+} ions and

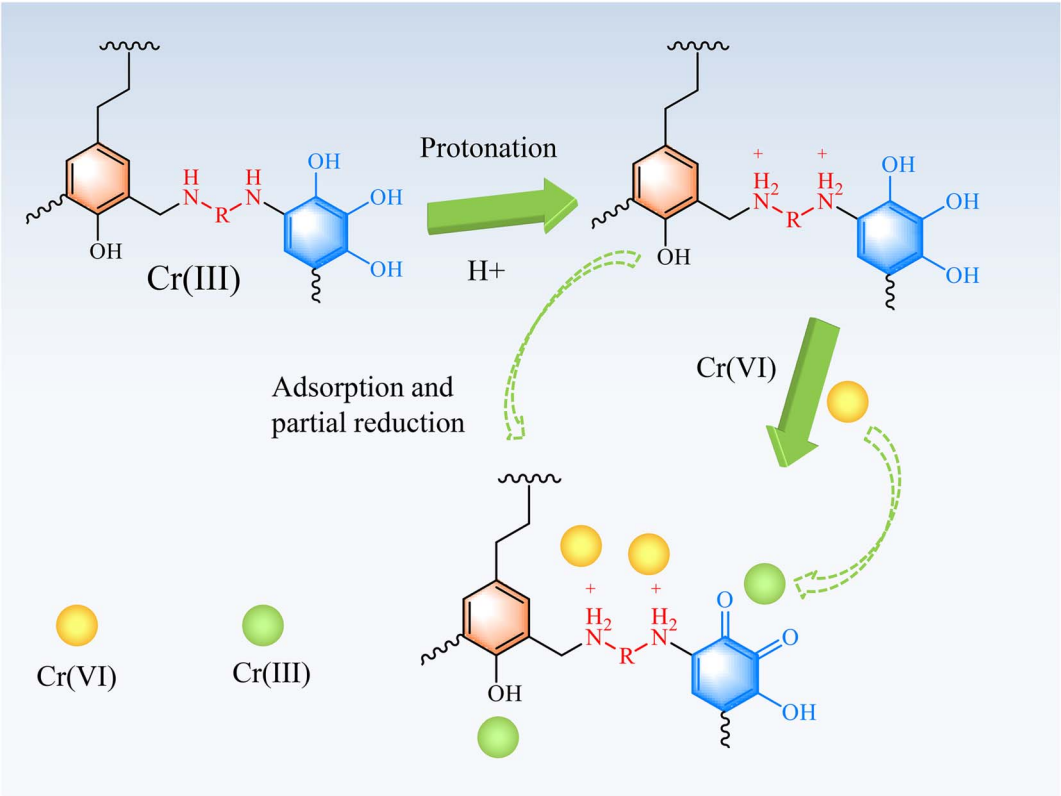

Fig. 9 Possible mechanism of Cr(VI) adsorption by AL-PTAP.

Cd^{2+} ions were added, respectively, in Cr(VI) ions at a molar ratio of 1 : 1. The adsorption capacity in the presence of K^{+} was 97.02% of the control experiment without competing ions, 94.86% in the presence of Cu^{2+} and 93.77% in the presence of Cd^{2+}. After adding these metal ions, AL-PTAP can still maintain a high adsorption capacity. This may be due to the protonation of amino groups in AL-PTAP in acidic solution (pH = 2) and these protonated groups generate electrostatic repulsion with metal cations. The repelled metal ions could not compete with Cr(VI) for adsorption sites and had little effect on the adsorption of Cr(VI) by AL-PTAP. As shown in Fig. 10b, Cl^{-}, NO_3^{-} and SO_4^{2-} were added, respectively, and the molar ratio of ions to Cr(VI) was 1 : 1. Cl^{-} and NO_3^{-} had little effect on the adsorption capacity and the adsorption capacity in the presence of Cl^{-} and NO_3^{-} was 97.02% and 92.58% of the control experiment, respectively. The effect of SO_4^{2-} on the adsorption capacity is relatively large and the adsorption capacity in the presence of SO_4^{2-} is 72.44%. This may be due to the stronger electrostatic

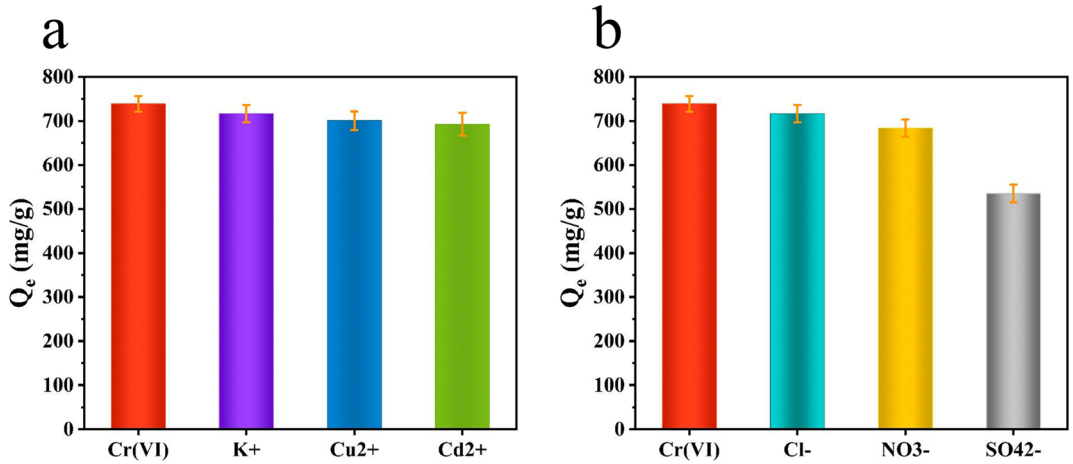

Fig. 10 Effects of competing ions on adsorption of Cr(VI) by AL-PTAP: (a) metal ions and (b) anions (condition: dose 0.025 g, initial Cr(VI) = 280 mg L^{-1}, pH = 2, 303.15 K, 24 h, the molar ratio of competing ions to Cr(VI) ions is 1 : 1).

Table 5 Maximum adsorption capacity of AL-PTAP and other reported adsorbents

Adsorbent	pH (°C)	Q_m (mg g^{-1})	Ref.
PHN	3	454.55	48
ZIF-8@PDA/PAN fibers	—	212.7	49
A series of micro–mesoporous activated carbons (ACs)	4.5	163.7	50
PEI-lignin particles	2	657.9	51
Fe_3O_4@mesoPDA	1.5	574.71	52
Lignin/GO composite nanospheres (LGNs)	2	368.78	53
Polydopamine microsphere (PDA-sphere)	3.8	200.2	54
Fluorescent lignin-based hydrogel	2	599.9	46
Cross-linked PEI	2	898.2	55
MoS_2@C-PAMA	—	800.0	56
AL-PTAP	2	769.2	Present study

force with the adsorption sites for divalent anions compared to monovalent ions (Cl^-, NO_3^-). Moreover, according to the research of Wang *et al.*,[47] the radius of SO_4^{2-} ion is closer to that of $HCrO_4^-$, so it has similar molecular size and hydration energy to $HCrO_4^-$. Therefore, compared with NO_3^- ions and Cl^- ions, SO_4^{2-} ions will more strongly affect the binding of $HCrO_4^-$ and adsorption sites, resulting in a decrease in the adsorption capacity. However, in the presence of SO_4^{2-}, the adsorption capacity is still 72.4% of the control experiment, which can be maintained at 535.2 mg g^{-1}. Therefore, AL-PTAP can still maintain high-capacity adsorption performance for Cr(VI) in complex wastewater.

3.12. Comparison of the removal capacity of different adsorbents for Cr(VI)

As shown in Table 5, the adsorption capacity of AL-PTAP is compared with other reported adsorbents. The AL-PTAP is better than most of others. The possible reasons may be owed to the structure of AL-PTAP. Alkali lignin and pyrogallol contains phenolic hydroxyl group, and tetraethylene pentamine contains amine group. Both of these two groups are hydrophilic and favour to adsorb Cr(VI). Besides, the aminated alkali lignin can cross-link pyrogallol to stable the AL-PTAP.

4. Conclusions

In this work, alkali lignin was modified by Mannich reaction and then it was linked by pyrogallol through catechol-amine reaction to prepare alkali lignin-based poly(tetraethylene pentamine-pyrogallol) (AL-PTAP). The AL-PTAP was utilized to adsorb Cr(VI) in water and the result was much higher than that of alkali lignin. The adsorption capacity of the AL-PTAP is as high as 769.2 mg g^{-1}, the removal percentage of Cr(VI) solution with a concentration of less than 140 mg L^{-1} can reach almost 100% and the removal percentage can reach almost 100% when the initial concentration less than 90 mg L^{-1} within 1 min. The adsorption behavior conforms to the pseudo-second-order kinetic model and the Langmuir isotherm model. Part of the toxic Cr(VI) was reduced to less toxic Cr(III) during the adsorption process. In conclusion, with the properties of high-capacity and fast adsorption, with the simple and low-cost preparation, AL-PTAP adsorbent is expected to improve the utilization value of alkali lignin in the treatment of Cr(VI) wastewater and has broad application prospects in the treatment of Cr(VI) wastewater.

Conflicts of interest

There are no conflicts to declare.

Acknowledgements

This work was supported by Natural Science Foundation of Shandong Province [ZR2020ME072, ZR2020ME082]; Youth Innovation Team Development Plan of Universities in Shandong Province (Grant No. 2021KJ056) and the Universities Twenty Foundational Items of Jinan City [2020GXRC027, 2021GXRC097, 2021GXRC068].

References

1 T. Sato, M. Qadir, S. Yamamoto, T. Endo and A. Zahoor, *Agric. Water Manag.*, 2013, **130**, 1–13.
2 Y. Wada, M. Florke, N. Hanasaki, S. Eisner, G. Fischer, S. Tramberend, Y. Satoh, M. T. H. van Vliet, P. Yillia, C. Ringler, P. Burek and D. Wiberg, *Geosci. Model Dev.*, 2016, **9**, 175–222.
3 X. Hu, J. Wen, H. Zhang, Q. Wang, C. Yan and L. Xing, *Chem. Eng. J.*, 2020, **391**, 123501.
4 İ. Duru, D. Ege and A. R. Kamali, *J. Mater. Sci.*, 2016, **51**, 6097–6116.
5 E. Brasili, I. Bavasso, V. Petruccelli, G. Vilardi, A. Valletta, C. Dal Bosco, A. Gentili, G. Pasqua and L. Di Palma, *Sci. Rep.*, 2020, **10**, 1920.
6 A. K. Mallik, M. A. Moktadir, M. A. Rahman, M. Shahruzzaman and M. M. Rahman, *J. Hazard. Mater.*, 2022, **423**, 127041.
7 D. M. Guo, Q. D. An, Z. Y. Xiao, S. R. Zhai and D. J. Yang, *Carbohydr. Polym.*, 2018, **202**, 306–314.
8 N. Sharma, K. K. Sodhi, M. Kumar and D. K. Singh, *Environ. Nanotechnol. Monit. Manag.*, 2021, **15**, 10388.
9 R. M. Rego, G. Sriram, K. V. Ajeya, H. Y. Jung, M. D. Kurkuri and M. Kigga, *J. Hazard. Mater.*, 2021, **416**, 125941.
10 Z. Y. Kong, Y. J. Du, J. F. Wei, H. Zhang and L. W. Fan, *J. Colloid Interface Sci.*, 2021, **588**, 749–760.

11 M. Jafarzadeh, *ACS Appl. Mater. Interfaces*, 2022, **14**, 24993–25024.
12 R. Verma, P. K. Maji and S. Sarkar, *J. Ind. Eng. Chem.*, 2022, **111**, 147–154.
13 D. F. Wang, Z. Q. Zong, J. H. Ye, Q. C. Wu, X. J. Zhang, Z. Y. Wu, J. Zhang, H. Xu and D. Q. Cai, *Chemosphere*, 2022, **294**, 133803.
14 W. H. Yu, Z. Q. Gan, J. R. Wang, Y. Zhao, J. Han, L. F. Fang, X. Z. Wei, Z. L. Qiu and B. K. Zhu, *J. Membr. Sci.*, 2021, **639**, 119756.
15 S. H. Park, S. S. Shin, C. H. Park, S. Jeon, J. Gwon, S. Y. Lee, S. J. Kim, H. J. Kim and J. H. Lee, *J. Hazard. Mater.*, 2020, **394**, 122512.
16 H. X. Liang, W. Ding, H. W. Zhang, P. Peng, F. Peng, Z. C. Geng, D. She and Y. Li, *Int. J. Biol. Macromol.*, 2022, **204**, 310–320.
17 H. Lee, S. M. Dellatore, W. M. Miller and P. B. Messersmith, *Am. Assoc. Adv. Sci.*, 2007, **318**, 426–430.
18 Q. Liu, Q. Z. Liu, B. S. Liu, T. Hu, W. L. Liu and J. S. Yao, *J. Hazard. Mater.*, 2018, **352**, 27–35.
19 E. Manarin, F. Corsini, S. Trano, L. Fagiolari, J. Amici, C. Francia, S. Bodoardo, S. Turri, F. Bella and G. Griffini, *ACS Appl. Polym. Mater.*, 2022, **4**, 3855–3865.
20 R. Penalva, A. L. Martinez-Lopez, C. Gamazo, C. J. Gonzalez-Navarro, C. Gonzalez-Ferrero, R. Virto-Resano, A. Brotons-Canto, A. I. Vitas, M. Collantes, I. Penuelas and J. M. Irache, *Food Hydrocoll.*, 2023, **136**, 108213.
21 J. Amici, C. Torchio, D. Versaci, D. Dessantis, A. Marchisio, F. Caldera, F. Bella, C. Francia and S. Bodoardo, *Polymers*, 2021, **13**, 1625.
22 S. Trano, F. Corsini, G. Pascuzzi, E. Giove, L. Fagiolari, J. Amici, C. Francia, S. Turri, S. Bodoardo, G. Griffini and F. Bella, *ChemSusChem*, 2022, **15**, e202200294.
23 G. Arias-Ferreiro, A. Ares-Pernas, A. Lasagabaster-Latorre, M. S. Dopico-Garcia, P. Ligero, N. Pereira, P. Costa, S. Lanceros-Mendez and M. J. Abad, *Adv. Mater. Technol.*, 2022, **7**, 2101503.
24 J. C. de Haro, C. Allegretti, A. T. Smit, S. Turri, P. D'Arrigo and G. Griffini, *ACS Sustainable Chem. Eng.*, 2019, **7**, 11700–11711.
25 L. N. Tan, N. C. T. Nguyen, A. M. H. Trinh, N. H. N. Do, K. A. Le and P. K. Le, *Sep. Purif. Technol.*, 2023, **304**, 122415.
26 A. B. Albadarin, A. H. Al-Muhtaseb, N. A. Al-laqtah, G. M. Walker, S. J. Allen and M. N. M. Ahmad, *Chem. Eng. J.*, 2011, **169**, 20–30.
27 Z. X. Song, W. Li, W. T. Liu, Y. Yang, N. N. Wang, H. J. Wang and H. Y. Gao, *RSC Adv.*, 2015, **5**, 13028–13035.
28 D. Kai, M. J. Tan, P. L. Chee, Y. K. Chua, Y. L. Yap and X. J. Loh, *Green Chem.*, 2016, **18**, 1175–1200.
29 A. Naseer, A. Jamshaid, A. Hamid, N. Muhammad, M. Ghauri, J. Iqbal, S. Rafiq, S. Khuram and N. S. Shah, *Z. Phys. Chem.*, 2019, **233**, 315–345.
30 M. Li, C. Tang, S. Fu, K. C. Tam and Y. Zong, *Int. J. Biol. Macromol.*, 2022, **216**, 860–870.
31 L. An, C. L. Si, J. H. Bae, H. Jeong and Y. S. Kim, *Int. J. Biol. Macromol.*, 2020, **159**, 222–230.
32 W. J. Yang, H. Ding, G. C. Qi, J. Q. Guo, F. Xu, C. C. Li, D. Puglia, J. Kenny and P. M. Ma, *Biomacromolecules*, 2021, **22**, 2693–2701.
33 C. G. Boeriu, D. Bravo, R. J. A. Gosselink and J. E. G. van Dam, *Ind. Crops Prod.*, 2004, **20**, 205–218.
34 T. Li, S. Y. Lu, Z. Q. Wang, M. J. Huang, J. Yan and M. Z. Liu, *Sci. Total Environ.*, 2021, **765**, 142745.
35 Z. Y. Peng, Y. B. Zou, S. Q. Xu, W. B. Zhong and W. T. Yang, *ACS Appl. Mater. Interfaces*, 2018, **10**, 22190–22200.
36 A. M. Omer, R. E. Khalifa, Z. H. Hu, H. Zhang, C. Liu and X. K. Ouyang, *Int. J. Biol. Macromol.*, 2019, **125**, 1221–1231.
37 J. Shang, Y. Guo, D. He, W. Qu, Y. Tang, L. Zhou and R. Zhu, *J. Hazard. Mater.*, 2021, **416**, 125706.
38 Q. H. Li, M. Dong, R. Li, Y. Q. Cui, G. X. Xie, X. X. Wang and Y. Z. Long, *Carbohydr. Polym.*, 2021, **253**, 117200.
39 J. Geng, L. Lin, F. Gu and J. M. Chang, *Ind. Crops Prod.*, 2022, **177**, 114522.
40 X. S. Wang, L. F. Chen, F. Y. Li, K. L. Chen, W. Y. Wan and Y. J. Tang, *J. Hazard. Mater.*, 2010, **175**, 816–822.
41 S. Jamshidifard, S. Koushkbaghi, S. Hosseini, S. Rezaei, A. Karamipour, A. J. Rad and M. Irani, *J. Hazard. Mater.*, 2019, **368**, 10–20.
42 Y. L. Li, X. Chen, L. Liu, P. Liu, Z. Z. Zhou, T. L. Huhe, Y. Q. Wu and T. Z. Lei, *J. Anal. Appl. Pyrolysis*, 2022, **162**, 105449.
43 D. Park, Y. S. Yun, H. W. Lee and J. M. Park, *Bioresour. Technol.*, 2008, **99**, 1141–1147.
44 Y. Zhang, Q. Liu, W. Ma, H. Liu, J. Zhu, L. Wang, H. Pei, Q. Liu and J. Yao, *J. Colloid Interface Sci.*, 2022, **609**, 825–837.
45 X. Shi, Y. Qiao, X. An, Y. Tian and H. Zhou, *Int. J. Biol. Macromol.*, 2020, **159**, 839–849.
46 H. Yuan, J. Peng, T. Ren, Q. Luo, Y. Luo, N. Zhang, Y. Huang, X. Guo and Y. Wu, *Sci. Total Environ.*, 2021, **760**, 143395.
47 W. W. Wang, J. B. Zhou, G. Achari, J. G. Yu and W. Q. Cai, *Colloids Surf. A: Physicochem. Eng. Asp.*, 2014, **457**, 33–40.
48 J. Li, S. Chen, H. Xiao, G. Yao, Y. Gu, Q. Yang and B. Yan, *New J. Chem.*, 2020, **44**, 12785–12792.
49 X. Yang, Y. H. Zhou, Z. J. Sun, C. H. Yang and D. Y. Tang, *New J. Chem.*, 2021, **45**, 15503–15513.
50 J. M. Zhao, L. H. Yu, F. Zhou, H. X. Ma, K. Y. Yang and G. Wu, *RSC Adv.*, 2021, **11**, 8025–8032.
51 H. W. Kwak, H. Lee and K. H. Lee, *Chemosphere*, 2020, **239**, 124733.
52 Q. Yang, H. L. Wang, F. B. Li, Z. Dang and L. J. Zhang, *J. Mater. Chem. A*, 2021, **9**, 13306–13319.
53 Z. Yan, T. Wu, G. Fang, M. Ran, K. Shen and G. Liao, *RSC Adv.*, 2021, **11**, 4713–4722.
54 Q. Zhang, Y. Li, Q. Yang, H. Chen, X. Chen, T. Jiao and Q. Peng, *J. Hazard. Mater.*, 2018, **342**, 732–740.
55 X. X. Shi, Y. Y. Qiao, X. X. An, Y. Y. Tian and H. F. Zhou, *Int. J. Biol. Macromol.*, 2020, **159**, 839–849.
56 F. F. Yu, W. K. Song, Z. L. Wu, W. X. Chen, J. P. Cui and Y. Y. Yao, *Sep. Purif. Technol.*, 2022, **294**, 121188.